

Rapid Defect Detection for Spacecraft in Infrared Reconstructed Images Using Image Mosaic Technique[★]

Kuo Zhang^{*} Chun Yin^{*} Yu-hua Cheng^{*} Xuegang Huang^{**}
Sara Dadras^{***} Xuan Gou^{*}

^{*} School of Automation Engineering, University of Electronic Science and Technology of China, Chengdu 611731, P. R. China (e-mail: yinchun.86416@163.com, chunyin@uestc.edu.cn).

^{**} Hypervelocity Aerodynamics Institute, China Aerodynamics Research & Development Center, Mianyang 621000, P. R. China.

^{***} Electrical and Computer Engineering Department, Utah State University, Logan, UT 84321, USA.

Abstract: In order to satisfy the real-time and large scale requirement of spacecraft non-destructive testing using optical pulsed thermography, in this research, we propose a novel approach based on image mosaic technique which can create large scale or panoramic image mosaics from a set of ordered infrared reconstruction images with overlapping areas for defect detection. First, infrared reconstruction images are extracted from the original thermal video stream by the ICA method based on the idea of blind source signal processing. Then for this research's special mosaic object, a fast and accurate registration scheme is proposed. Abundant scale rotation invariant feature points are quickly obtained by using the hybrid feature detector and descriptor. Moreover, the feature matching process is realized by applying two-way FLANN and MSAC, parameters of the geometric transformation matrix are estimated by MSAC, and image mosaic is realized according to the geometric transformation model. The experimental results convinced the validity and efficiency of the proposed method.

Keywords: Hypervelocity impact (HVI), Optical pulsed thermography, Defect detection, Blind source signal processing, Image mosaic

1. INTRODUCTION

At present, the risk of hypervelocity impact (HVI) caused by meteoroid/orbital debris (M/OD) has become one of the main threats to spacecraft space activities, and will have more serious impact on spacecraft, such as the damage caused by surface craters and internal embedded impurities(Price et al. (2013),Huang et al. (2016),Huang et al. (2020)). Considering the randomness of the M/OD impact event, the impact and extent of the impact are uncertain, which will lead to complex and variable damage, so the detection of potential damage to spacecraft is an important research direction. In order to obtain an effective M/OD impact evaluation, OPT(optical pulsed thermography) as a *NDT&E* (non-destructive testing and evaluation) method is widely used due to its high efficiency, low loss and high safety. In the optical pulsed thermography detection system, thermal radiation changes caused by defects lead to different temperature variety rates in different detection areas of the testing area(Yin et al. (2019),Ibrahim and Zhuang (2017)). So in this paper, the optical pulsed thermography is implemented in the defects

[★] This work was supported by National Basic Research Program of China (Grant No. 61873305, 61671109 and U1830207) and Sichuan Science and Technology Plan Project (Grant 2019YJ0199, 2018JY0410). (Corresponding author: Chun Yin)

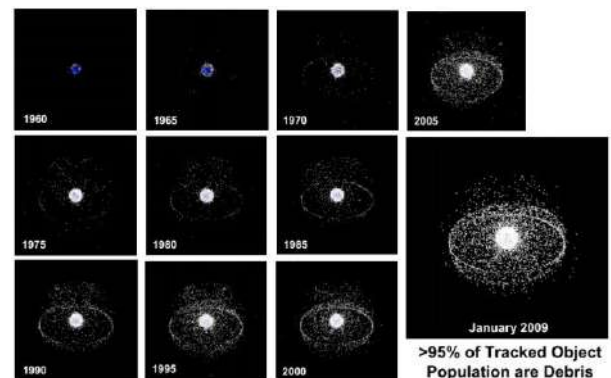


Fig. 1. Development of space debris environment in Huang et al. (2020).

detection of spacecraft. Researchers have made valuable contributions about processing data in OPT, which can be applied in *NDT&E*. Duan et al. (2013) utilized a quantitative method for probability of detection analysis based on optical pulsed thermography. Zhang et al. (2018) used optical excitation thermography for inspecting multilayer carbon fibre defects for the first time.

Nevertheless, the above methods are quantitative research and systematic improvement of detection methods for

smaller defect areas. For the spacecraft size and single detection area is limited, it is necessary to understand the defect information (such as distribution and extent) of a large range of detection area firstly. Separating two-dimensional image information from the collected infrared video stream so as to evaluate the damage conveniently and effectively. Similar to remote sensing image processing, mosaics can be applied to detect the wide range of surface of the spacecraft (Bell et al. (2015)). Image registration is one of the key techniques for image mosaic and is the basis of image mosaic (Jung et al. (2018), Wang et al. (2018)). In recent years, scholars have proposed many feature extraction algorithms and the corresponding improved algorithms. From the earliest Moravec, to Harris, to SIFT, SUSAN, and SURF algorithms (Lowe (2004), Bay et al. (2008), Harris and Stephens (1988)), it can be said that feature extraction algorithms are emerging. Various improved algorithms such as GLOH, BP-SIFT, MM-SURF, etc (Zhu et al. (2013), Mikolajczyk and Schmid (2005), Zhao et al. (2014)), also achieve their own strengths. However, feature extraction is only a small part in the whole non-destructive testing system, if the algorithm does not perform well in real time, it will reduce the overall performance of the testing system.

Aiming at obtaining images of research significance from the original data, the reconstructed image that highlights specific region information can be extracted by ICA (Khan et al. (2008), Rajic (2002)). In order to meet the purpose of real-time detection and considering the special mosaic object, a hybrid feature extraction scheme is proposed. The FAST algorithm is used for feature detection and the SURF feature descriptor is generated so that the mosaic algorithm still has rotation and scale invariance. Then, the MSAC (M-estimator Sample Consensus) algorithm is used to eliminate the error matching points and estimate the geometric transformation model to realize the image mosaic process (Torr and Zisserman (2000)). The experimental results demonstrate the capabilities and potential application value of the algorithm.

2. PROBLEM STATEMENT

The hypervelocity impacts should become inevitable for spacecraft, because of the micro meteoroids and space debris particles that couldn't be completely detected and prevented. Hence, it is necessary to investigate the impact damage evolution. Moreover, a simple micro-scale M/OD hypervelocity impact could lead to surface/internal-damages of thermal protection materials, that would affect the normal operation of the spacecraft. Therefore, it is necessary to detect and evaluate the HVI impact damages with some effective non-destructive testing technologies firstly.

In addition to not damaging the original item, the defect detection method by OPT is fast and efficient. The spatial thermal responses of detection area are recorded by IR camera as an infrared thermal video. Although the thermal video is rich in information, the calculation of video information processing is more complex. Furthermore, for the large range of requirements for spacecraft defect detection, a single video can only reflect a small part of the testing region and the video information of each

region cannot be easily united. If the image that highlights the surface and internal defects of the spacecraft can be extracted from the thermal video stream, the 2D image is easier to be processed and interacted with images from other regions, which can greatly speed up the detection efficiency and carry out subsequent follow-up detailed research on defects. The schematic diagram of the non-destructive testing method is shown as Fig. 2. After the infrared non-destructive testing of the spacecraft, it is assumed that for a certain defect area detected, n local regions are detected. The thermal video obtained for each region are processed to extract images, which are prominent defects and prominent background portions determined by typical thermal responses, respectively.

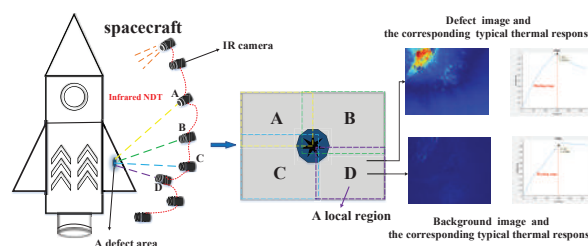


Fig. 2. Schematic diagram of infrared nondestructive testing of spacecraft

Spacecraft is huge and complex in surface structure, coupled with the subsurface defects that cannot be observed directly. In order to make the HVI damage evaluation of the spacecraft comprehensive and intuitive, the extracted images highlighting the defect information are applied to the image mosaic technology. And the goal of the mosaic is to preliminarily evaluate the damage degree and understand the location distribution of the detected area according to the mosaic images, so as to realize the preliminary defect localization and judgment of the spacecraft damage assessment. Different from mosaic method of natural visible light image and small object image, in terms of the special infrared thermal image object, the corresponding effective and practical mosaic algorithm are needed.

3. INTRODUCTION OF PROPOSED ALGORITHM

For image sequence acquired by each infrared video, the reconstructed image is extracted by using the ICA algorithm. It should be pointed out that for the local region with defects, the reconstructed image can highlight the defect information. Then, the image mosaic scheme proposed in this paper is applied to the reconstructed images of local regions. Firstly, the hybrid feature detector and descriptor is adopted to ensure the fastness and rotation and scale invariance of feature extraction. Then, the two-way FLANN algorithm is utilized to perform the feature rough matching process and the MSAC algorithm is used to eliminate the mismatching point pairs and estimate the geometric transformation matrix model. Finally, according to the geometric transformation model, the affine transformation is realized to get the mosaic result. The details of the steps of the proposed registration scheme are presented in the following sections and the algorithm flow chart of this paper is shown in Fig. 3.

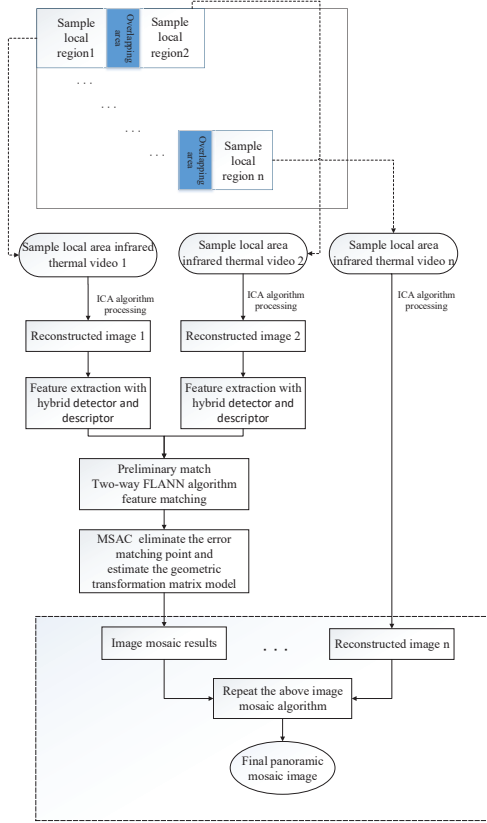


Fig. 3. the flow chart of the image mosaic algorithm used in this paper

3.1 Reconstructed image obtained by ICA algorithm

Different independent feature areas show different typical thermal responses, which can help us extract independent signal images and we call these typical independent signal images as reconstructed images. Combining the ICA mathematical model and the relationship between the signal characteristics of each defect area and the thermal video signal, the reconstructed image of each region can be extracted. Based on above analysis, the goal of ICA is to separate several independent components from the blind source signals of original image sequences. The basic mathematical model of ICA in OPT can be described as:

$$Q'(t) = \sum_{i=1}^L m_i P'_i(t) \quad (1)$$

$m_i (i = 1, 2, 3, \dots, L)$ is the mixing vector that describes the contribution of the i^{th} position to the recorded thermography image. L denotes the number of desired reconstructed images. $P'_i(t)$ denotes the independent image signal generated by the area of position i at time t with dimensional p by q . In this study, p by q are determined by the infrared camera sensor array with setting as $p = 512, q = 640$. $Q'(t)$ represents the data of the preprocessed initial image sequence. The data is discretized and decomposed to obtain a new matrix, such that continuous transient slices of length N can be chopped out of a set of image sequences from t to $t + N - 1$. $Q'(t) = [vec(Q'(t)), vec(Q'(t+1)), \dots, vec(Q'(t+N-1))]^T$. The reconstructed image sequence is then described as a linear combination of the signals generated by the independent

areas such that:

$$Q(t) = MP(t) \quad (2)$$

where mixing matrix $M = [m_1, m_2, \dots, m_L]$ and m_i is the i^{th} mixing vector of the independent area. $P(t) = [vec(P_1(t)), vec(P_2(t)), \dots, vec(P_L(t))]^T$. Assuming that $L = N$ and matrix M is full rank so that we can derive another representation from this :

$$P(t) = WQ(t) \quad (3)$$

where $W = M^{-1}$ is inverse transforms. The purpose of the ICA algorithm is to search for the linear transformation that make the components as statistically independent as possible. Maximizing the marginal densities of the transformed coordinates for the given training data, which is

$$\hat{W} = \arg \max_w \prod_t \Pr(Q(t)|W) = \arg \max_w \prod_t \prod_i \Pr(p_i(t)) \quad (4)$$

where $p_i(t) = vec(P_i(t))$ and $\Pr(\cdot)$ is its corresponding probability. To solve equation (4) we use PCA whiten to $Q(t)$ by applying singular value decomposition of the following equation.

$$Q(t)^T = U_{R \times R} \Sigma_{R \times N} V^T_{N \times N} \quad (5)$$

where $R = p \times q$, $U_{R \times R}$ and $V^T_{N \times N}$ are the orthogonal matrices, $\Sigma_{R \times N}$ contain the singular values and the columns of $U_{R \times R}$ represented by the PCA basis vectors. Applying PCA method to achieve dimensionality reduction, choosing $L \leq N$ thus the $U_{R \times L}$ basis vectors are selected and determined by the information contained in the non-zero singular values. The basis vectors obtained by PCA method are only uncorrelated but not statistically independent. Next, the independent basis vectors must be derived by employing ICA algorithm where the PCA basis vectors $U_{R \times L}$ are referenced as the observations in ICA, namely

$$U^T_{R \times L} = M_{L \times L} P_{L \times R}(t) \quad (6)$$

ICA estimates the demixing matrix \hat{W} that is an approximation of the inverse of the original mixing matrix. The independent components can be obtained

$$\hat{P}_{L \times R}(t) = \hat{W}_{L \times L} U^T_{R \times L} \quad (7)$$

For each estimated ICs, the reconstruction process of the independent component image sequences generated by the i^{th} area can be expressed as

$$\hat{P}_i = \hat{m}_i \hat{p}_i(t)^T \quad (8)$$

where \hat{m}_i is the i^{th} vector of estimated \hat{M} . The pseudo-inverse matrix of \hat{W} describes the mixing matrix \hat{M} building with mixing vectors. \hat{P}_i is the obtained image sequence of the feature region highlighting each independent component.

3.2 Hybrid feature detector and descriptor

The FAST detection algorithm is an algorithm with a fast detection speed, which is an order of magnitude faster than the SURF algorithm, but does not have scale and rotation invariance. So in this paper, we choose the feature detector based on FAST combined with the SURF descriptor to make the feature points have anti-rotation characteristics at the same time.

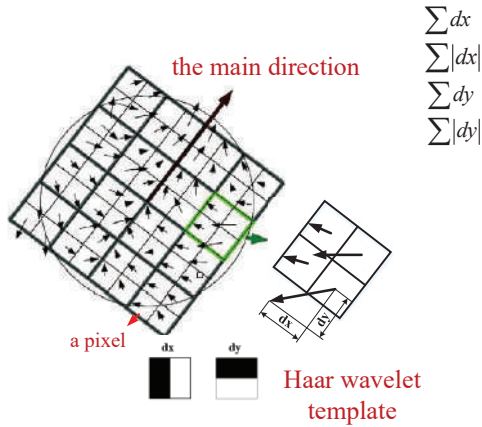


Fig. 4. Schematic diagram of SURF algorithm

3.2.1 FAST feature detector FAST (Features accelerated from Segment Test) algorithm is widely applied due to its fast detection speed and simple algorithm structure. The main method of FAST algorithm is to use a 16-pixel circle (radius is 3 pixels) to determine whether the center pixel is a corner or non-corner. It is the result of comparing the intensity of all these pixels from the center pixel, forming a corner. If at least 12 of the 16 pixels are considered to be distinct, the center pixel will be defined as a corner. That is, the equation (9) is satisfied:

$$D = \begin{cases} 1 & \text{if } |I(x) - I(p)| > \varepsilon \\ 0 & \text{else} \end{cases} \quad (9)$$

where: $I(x)$ represents the gray value of a pixel point; $I(p)$ represents the gray value of the target pixel p ; ε is a predetermined threshold. If there are n (n is greater than a given threshold ε) consecutive pixels, and the equation (9) are fully satisfied, $D = 1$, which is the corner point, and the center pixel is the feature point. The threshold is initially chosen to be 12, which eliminates non-corner points and has the advantage of faster speeds to meet real-time matching needs.

3.2.2 SURF Feature descriptor In order to ensure that the feature descriptor has rotation invariance, it is necessary to assign a main direction to all the feature points detected by FAST. The wavelet response of X and Y directions is obtained by Haar wavelet template, which is shown in Fig. 4. Because we calculate the Haar wavelet response of the X , Y direction for each point, the sum of the Haar wavelet responses included in this sector is a vector. And the vector obtained by rotating the sector for a circle is recorded. The angle corresponding to the vector length is denoted as the direction of the feature point.

After determining the main direction, the next step is to generate a feature descriptor. As shown in Fig. 4, in the square window with the feature point as the center 20σ as the side length. The $20\sigma \times 20\sigma$ window is divided into 4×4 sub-windows, each cell has $5\sigma \times 5\sigma$ pixels, and 25 samples are taken to obtain the wavelet response value in the main direction $\sum dy$ and the wavelet response value perpendicular to the main direction $\sum dx$. Get the vector of each sub-block $V = [\sum dx, \sum |dx|, \sum dy, \sum |dy|]$. Counting the vector of 4×4 sub-block regions obtains a 64-dimensional vector, which is the feature descriptor.

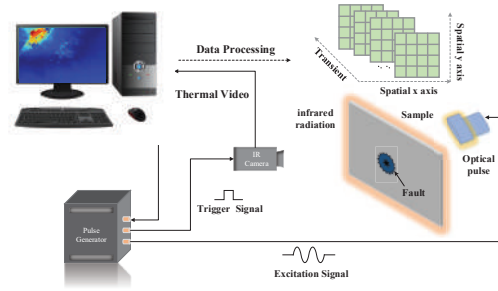


Fig. 5. The experimental schematic diagram

3.3 Feature matching and transformation model estimation

In order to improve the correct rate and speed of matching, the two-way FLANN algorithm is first used to find the matching point pairs with the nearest neighbor distance. Euclidean distance is used as a measure of similarity. Matched points that have been initially screened are further purified by the m-estimator sample consensus (MSAC) algorithm.

3.3.1 two-way FLANN algorithm Since the feature vector is a high-dimensional vector, conventional matching methods require a huge amount of computation. And the FLANN (fast library for approximate nearest neighbors) based on the accuracy of user input and high-dimensional data automation is applied, which makes the search speed significantly improved. In order to obtain reliable and accurate unique matching point pairs, this paper uses the two-way FLANN algorithm. Due to the fast speed of the FLANN matching algorithm, the two-way FLANN matching algorithm improves the matching accuracy by wasting a small amount of time, which also provides more accurate matching point pairs for the subsequent algorithm of removing mismatches and speeds up the following stitching algorithm.

3.3.2 MSAC algorithm The MSAC algorithm is a method of searching for inner points. It uses the inherent constraints of the feature point set to remove the wrong matching point pairs. Compared with the more basic RANSAC algorithm, MSAC uses M-estimator to estimate the weight of the data, instead of simply assigning a zero value to the inner points, so that the accuracy of the model is further increased. Based on RANSAC, MSAC improves the cost function with the following expression:

$$p(e_i^2) = \begin{cases} e_i^2 & e_i^2 < T^2 \\ cons & e_i^2 \geq T^2 \end{cases} \quad (10)$$

$$C = \sum_i p(e_i^2). \quad (11)$$

where e_i^2 represents the difference between the i th actual value of the data and the theoretical value, $p(e_i^2)$ is the data error weight and C is the overall error of the model sought, called the cost function. T^2 is a predetermined threshold. The value of C is compared after the end of the iterative process, and the minimum value of C is taken as the best model. Compared with RANSAC, the calculations are completely consistent, but the accuracy is increased and the convergence speed is faster. Then suppose a pair of correct matching points X and X' exist in the reference

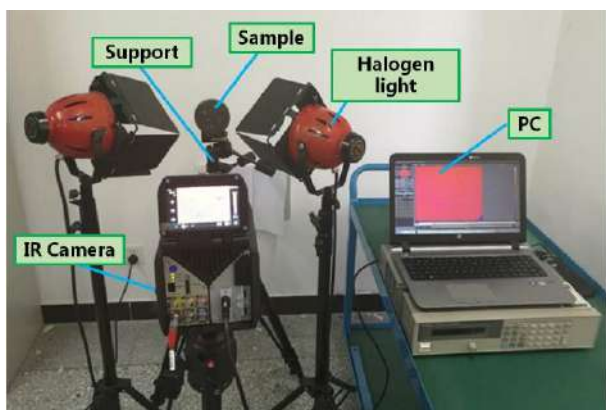


Fig. 6. Experimental set-up

image and the image to be spliced. The corresponding homogeneous coordinate transformation is:

$$X' \sim FX = \begin{bmatrix} f_0 & f_1 & f_2 \\ f_3 & f_4 & f_5 \\ 0 & 0 & 1 \end{bmatrix} X \quad (12)$$

Where: F is a 3×3 matrix, that is, the geometric transformation matrix. The six elements of the matrix $f_0 \sim f_5$ are unknown. The coordinate transformation between images can be completed by solving the parameters. The purpose of the MSAC algorithm is to find all the correct matching points and obtain the most accurate geometric transformation matrix.

4. EXPERIMENTAL RESULTS AND DISCUSSIONS

4.1 Experiment setup

In our experiments, an optical pulse is generated and the surface temperature of the sample is recorded in one time and the experimental schematic diagram is shown in Fig. 5. Heat radiation is generated by the optical excitation source. Computer-controlled pulse generators generate excitation and trigger signals to initiate optical excitation source heating and infrared data acquisition. We set the heating time to 0.1s for observation and study.

After these hypervelocity impact tests, the sample with impact damages are collected for the further research of detecting defects. The test piece is thermally excited, a thermal image sequences is collected by using the infrared thermal camera with a resolution of 512×640 , as shown in Fig. 6. The sample is divided into four local regions (A1-A4) containing overlapping parts for infrared video acquisition. The reconstructed images of each local region were obtained by ICA algorithm section above.

4.2 Comparison and analysis

Aiming at the special mosaic object, the mosaic scheme proposed in the theoretical part of this paper, the conventional SIFT-RANSAC (the rough match processing is a one-way matching) and the SURF-RANSAC scheme were compared and analyzed. Fig. 7 shows the result of feature detection and feature matching removing mismatches for A3 and A4. As can be seen from the Fig. 7, there is no mismatch in the method of this paper, and the correct number of matches is obviously the most. At the same

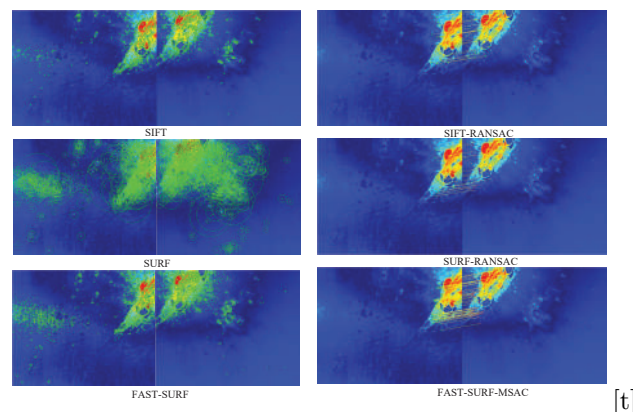


Fig. 7. The contrastive result of feature detection and feature matching removing mismatches

time, the matching time is much shorter, less than half of the other methods. The statistical data in Table 1 shows the specific experimental data comparison.

4.3 Image mosaic results

For applying the mosaic scheme proposed in this paper, sample A is divided into four local regions containing overlapping parts. First, the region A1 and A2 was spliced to obtain the mosaic results of A1-A2, then spliced with A3 to obtain the mosaic results of A1,2-A3, and finally spliced with A4 to obtain the final mosaic results A1,2,3-A4. As can be seen from the Table 2, the overall effect is very good, which can directly observe the defect parts and facilitate the follow-up research on the defect parts.

5. CONCLUSION

In this research, we propose a new image mosaic approach for defect detection of and evaluation spacecraft in optical pulsed thermography. The preliminary judgment of impact evaluation using 2D images is realized, which is more intuitive and convenient. Our future work will focus on detailed analysis of the mosaic images, including defect classification and other quantitative analysis.

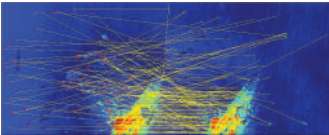
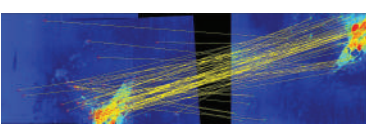
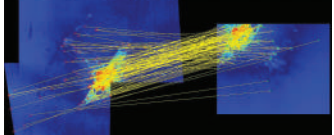
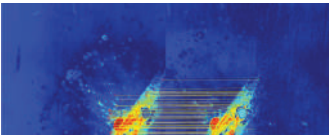
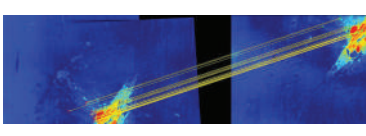
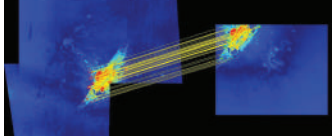
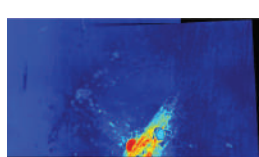
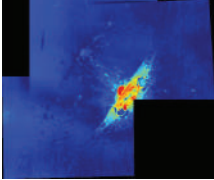
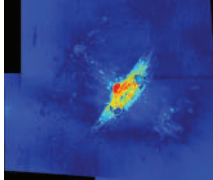
REFERENCES

- Bay, H., Ess, A., Tuytelaars, T., and Gool, L.V. (2008). Speeded-up robust features (surf). *Computer Vision and Image Understanding*, 110(3), 346 – 359.
- Bell, G., Neal, S., and Medcalf, K. (2015). Use of remote sensing to produce a habitat map of norfolk. *Ecological Informatics*, 30, 293 – 299.
- Duan, Y., Huebner, S., Hassler, U., Osman, A., Ibarra-Castaneda, C., and Maldague, X.P. (2013). Quantitative evaluation of optical lock-in and pulsed thermography for aluminum foam material. *Infrared Physics & Technology*, 60, 275 – 280.
- Harris, C. and Stephens, M. (1988). A combined corner and edge detector. *Proceedings 4th Alvey Vision Conference*, 1988, 147–151.
- Huang, X., Yin, C., Huang, J., Wen, X., Zhao, Z., Wu, J., and Liu, S. (2016). Hypervelocity impact of TiB2-based composites as front bumpers for space shield applications. *Materials & Design*, 97, 473 – 482.

Table 1. Data comparison of various registration schemes

Basis	Feature extraction time /s	Number of feature extraction	Feature matching time /s	Number of feature matches	Correct matching number
SIFT-RANSAC	1.351472	667/891	1.130706	1048	17
SURF-RANSAC	0.040546	1161/986	1.151549	83	31
method proposed	0.004685	1972/1936	0.475716	101	52

Table 2. Specific display of image mosaic

Object	Sample A1-A2	Sample A1,2-A3	Sample A1,2,3-A4
Initial feature matching			
Remove mismatches			
The final result			

- Huang, X., Yin, C., Ru, H., Zhao, S., Deng, Y., Guo, Y., and Liu, S. (2020). Hypervelocity impact damage behavior of B4C/Al composite for MMOD shielding application. *Materials & Design*, 186, 108323.
- Ibrahim, M.E. and Zhuang, W.Z. (2017). Nondestructive inspection of fatigue crack propagation beneath supersonic particle deposition coatings during fatigue testing. *International Journal of Fatigue*, 102, 149 – 157.
- Jung, S., Song, S., Chang, M., and Park, S. (2018). Range image registration based on 2d synthetic images. *Computer-Aided Design*, 94, 16 – 27.
- Khan, A., Vrabie, V., Mars, J., Girard, A., and D'Urso, G. (2008). A source separation technique for processing of thermometric data from fiber-optic dts measurements for water leakage identification in dikes. *Sensors Journal, IEEE*, 8, 1118 – 1129.
- Lowe, D.G. (2004). Distinctive image features from scale-invariant keypoints. *International Journal of Computer Vision*, 60(2), 91–110.
- Mikolajczyk, K. and Schmid, C. (2005). A performance evaluation of local descriptors. *IEEE Transactions on Pattern Analysis & Machine Intelligence*, 27(10), 1615–1630.
- Price, M., Solscheid, C., Burchell, M., Josse, L., Adamek, N., and Cole, M. (2013). Survival of yeast spores in hypervelocity impact events up to velocities of 7.4kms?1. *Icarus*, 222(1), 263 – 272.
- Rajic, N. (2002). Principal component thermography for flaw contrast enhancement and flaw depth characterization in composite structures. *Composite Structures*, 58(4), 521 – 528.
- Torr, P. and Zisserman, A. (2000). Mlesac: A new robust estimator with application to estimating image geometry. *Computer Vision and Image Understanding*, 78(1), 138 – 156.
- Wang, S., Quan, D., Liang, X., Ning, M., Guo, Y., and Jiao, L. (2018). A deep learning framework for remote sensing image registration. *ISPRS Journal of Photogrammetry and Remote Sensing*, 145, 148 – 164.
- Yin, C., Xue, T., Huang, X., Cheng, Y., Dadras, S., and Dadras, S., (2019). Research on damages evaluation method with multi-objective feature extraction optimization scheme for M/OD impact risk assessment. *IEEE Access*, 7, 98530 – 98545.
- Zhang, H., Robitaille, F., Grosse, C.U., Ibarra-Castaneda, C., Martins, J.O., Sfarra, S., and Maldague, X.P. (2018). Optical excitation thermography for twill/plain weaves and stitched fabric dry carbon fibre preform inspection. *Composites Part A: Applied Science and Manufacturing*, 107, 282 – 293.
- Zhao, D., Yang, Y., Ji, Z., and Hu, X. (2014). Rapid multimodality registration based on mm-surf. *Neurocomputing*, 131, 87 – 97.
- Zhu, Y., Cheng, S., Stankovic, V., and Stankovic, L. (2013). Image registration using bp-sift. *Journal of Visual Communication and Image Representation*, 24(4), 448 – 457.